Journal of Molecular Catalysis A: Chemical 302 (2009) 129–136

Contents lists available at ScienceDirect

Journal of Molecular Catalysis A: Chemical

journal homepage: www.elsevier.com/locate/molcata

Structure and energetics of hydrogen adsorption on Fe_3O_4(1 1 1)

Tao Yang[a], Xiao-Dong Wen[a], Chun-Fang Huo[a], Yong-Wang Li[a], Jianguo Wang[a], Haijun Jiao[a,b,*]

[a] State Key Laboratory of Coal Conversion, Institute of Coal Chemistry, Chinese Academy of Sciences, Taiyuan, Shanxi 030001, PR China
[b] Leibniz-Institut für Katalyse e.V. an der Universität Rostock, Albert-Einstein-Strasse 29a, 18059 Rostock, Germany

ARTICLE INFO

Article history:
Received 16 May 2008
Received in revised form 3 December 2008
Accepted 11 December 2008
Available online 24 December 2008

Keywords:
Hydrogen adsorption
Fe_3O_4
Catalysis
DFT

ABSTRACT

Hydrogen adsorption on the Fe_{tet1}- and Fe_{oct2}-terminated Fe_3O_4(1 1 1) surfaces has been computed at the level of density functional theory. At 2/5 monolayer (ML), the most favored hydrogen adsorption on the Fe_{tet1}-terminated surface is homolytic and dissociative on surface O atoms, while other adsorption modes become possible at higher coverages. On the Fe_{oct2}-terminated surface at 1/3 ML, hydrogen prefers to adsorb heterolytically and dissociatively on surface Fe and O atoms, while other adsorption modes become in close energy at 2/3 and 1 ML. The Fe_{tet1}-terminated surface is more favored than the Fe_{oct2}-terminated surface for hydrogen adsorption. The adsorption mechanism has been analyzed on the basis of the calculated local density of state.

1. Introduction

Magnetite (Fe_3O_4) has attracted much attention because of its unique properties and potential applications in electronics, magneto-recording and heterogeneous catalysis [1–7]. One of the representative examples is Fe_3O_4-catalyzed water–gas shift (WGS) reaction [8–11]. As iron carbides and iron phases, Fe_3O_4 [12–14] is one active phase in Fischer–Tropsch synthesis (FTS).

Experimental studies on water adsorption on different surfaces of Fe_3O_4 [15–17] indicated the formation of OH and H species bonded to the iron and oxygen atoms exposed on the topmost layer of the Fe_3O_4(1 1 1) surface, respectively. Weiss et al. [18–20] studied the adsorption of ethylbenzene and styrene on different iron oxide films. Adib et al. [21] studied CCl_4 adsorption on the Fe_3O_4(1 1 1)-(2 × 2) selvedge of α-Fe_2O_3(0 0 0 1). Lemire et al. [22] studied CO adsorption on the Fe_3O_4(1 1 1) films grown on a Pt(1 1 1) substrate. It is noted that in FTS and WGS the presence of hydrogen on a catalyst surface has a pronounced influence on its chemical and electrical properties as well as catalytic activity and reaction mechanism [23–25]. However, due to the fact that the standard methods, such as low-energy electron diffraction, X-ray photoelectron spectroscopy and Auger electron spectroscopy, are not sufficiently sensitive for H atom, there are few experimental results on hydrogen adsorption so far.

Quantum chemical methods have become new tools for studying the structure of active surfaces and determining reaction mechanisms. With recent developments, density functional theory (DFT) is capable of providing qualitative and, in many cases, quantitative insights into surface science and catalysis. DFT calculations on Fe_3O_4 structures have been carried out [26–28]. To understand the catalytic active and surface properties Huang et al. [29] have studied CO adsorption on the Fe_{tet1}- and Fe_{oct2}-terminations. Most recently, Grillo et al. [30] studied the surface structure and water adsorption by using spin-density functional theory and found that initial water adsorption is dissociative and saturates when all Fe sites are occupied by OH groups and H atoms bind to surface oxygen. In addition, the energetic aspects of the carburization process of the Fe_3O_4(1 1 1) surface have been computed [31]. To our knowledge, hydrogen adsorption on the Fe_3O_4 surface is still lacking. Recently we have studied hydrogen adsorption on the surfaces of iron and iron carbides because of their importance in FTS processes on the basis of DFT calculations [32,33].

In this work, we report a systematic DFT study on hydrogen adsorption on two different terminations (Fe_{tet1}- and Fe_{oct2}-termination) of the Fe_3O_4(1 1 1) surface for understanding the surface structure and activity, which are essential for the catalytic mechanism of WGS and FTS processes.

2. Methods and models

All calculations were done with the Cambridge Sequential Total Energy package (CASTEP) [34]. The Perdew–Burke–Ernzerhof (PBE) functional [35] within the generalized gradient approximation (GGA) [36] was used. Ionic cores were described by ultrasoft

* Corresponding author at: Leibniz-Institut für Katalyse e.V. an der Universität Rostock, Albert-Einstein-Strasse 29a, 18059 Rostock, Germany.
Tel.: +49 381 1281 135; fax: +49 381 1281 5000.
E-mail address: haijun.jiao@catalysis.de (H. Jiao).

1381-1169/$ – see front matter © 2008 Elsevier B.V. All rights reserved.
doi:10.1016/j.molcata.2008.12.009

pseudopotential [37], and the Kohn–Sham one-electron states were expanded in a plane wave basis set up to 300 eV. The error of the adsorption energy at the level of cutoff between 300 and 340 eV was within 0.02 eV. A Fermi smearing of 0.1 eV was used. Brillouin zone integration was approximated by a sum over special k points chosen using the Monkhorst–Pack scheme [38], and the k point of 0.05 $Å^{-1}$ spacing is utilized. The pseudopotential with partial core was used in spin-polarized calculation to include nonlinear core corrections [39]. Spin polarization having a major effect on the adsorption energies for magnetic systems [40] was included to correctly account the magnetic properties of Fe_3O_4. Without counting the adsorbate, the vacuum between the slabs was set to span a range of 10 Å to exclude the interaction of the slabs. The convergence criteria for the structure optimization and energy calculation were set to (a) a SCF tolerance of 2.0×10^{-6} eV/atom, (b) an energy tolerance of 2.0×10^{-5} eV/atom, (c) a maximum force tolerance of 0.05 eV/Å, and (d) a maximum displacement tolerance of 2.0×10^{-3} Å.

Since it is technically not possible to perform vibrational frequency calculations with CASTEP for characterizing the energy minimum structures, we have taken the following alternative strategy for making sure that the optimized structures to be energy minimums: (a) all possible initial orientations were considered; (b) no symmetry constrains were used; (c) free optimization of all initial positions converges to the same structure with the same energy; (d) CASTEP uses BFGS geometry optimization method to locate energy minimum structure.

Fe_3O_4 has a cubic inverse spinel structure with a lattice constant of 8.396 Å [41]. Fe_3O_4(1 1 1) is one predominant natural growth face and its catalyst activity is higher than that of other surfaces [42,43]. Cutting the Fe_3O_4(1 1 1) stacking sequence can generate six non-equivalent ideal bulk terminations and the termination with the less number of the dangling bond shows higher stability. A cleavage through the iron multilayer of the Fe_3O_4(1 1 1) stacking sequence gives two terminations with the least dangling bonds [44], i.e.; Fe_{tet1}- and Fe_{oct2}-terminated surface, and they have been proposed as the most stable terminations [22,26,45]. We choose them as the models to investigate the hydrogen adsorption. The very open structures of these two surfaces have exposed iron and oxygen atoms (Fe_{tet1} layer: Fe_{tet1} and O; Fe_{oct2} layer: Fe_{oct2}, Fe_{tet1} and O). Comparing the influence of the thickness (the error within 10%), we used a model system with eight layers, in which the top four layers were relaxed, and the bottom layers were fixed in their bulk position (Fig. 1). For the Fe_{tet1}-termination, the top two iron layers and two oxygen layers (2Fe/2O) were relaxed, and the bottom three iron layers and one oxygen layer (3Fe/O) were fixed (Fig. 1A). For the Fe_{oct2}-termination, the top three iron layers and one oxygen layer (3Fe/O) were relaxed, and the bottom three iron layers and one oxygen layer (3Fe/O) were fixed (Fig. 1B). The iron atoms of the uppermost layer are labeled as Fe_{tet1} and Fe_{oct2}, and the oxygen atoms of the second layer are signed as a, b, c and d, respectively.

For calculating the adsorption energy per H_2, $E_{ads} = [E(H/slab) - E(slab) - nE(H_2)]/n$ is utilized. Here, $E(H/slab)$ is the total energy for the slabs with adsorbed hydrogen, $E(slab)$ is the total energy of the bare slab of the surface, $E(H_2)$ is the total energy of free H_2, and n is the number of the adsorbed H_2. Therefore, the more negative the E_{ads}, the stronger the adsorption. The H coverage (θ_H) is defined as the number of the adsorbed H atoms over the number of the exposed Fe and O atoms on the surface. In our calculations, H_2 was initially oriented parallel to the surface, the initial parameters of H_2 atop the iron atoms was set to 1.75 Å for H–Fe bonds (from low-energy electronic diffraction [46]) and that of the surface oxygen (O–H) was 1.3 Å, while the H–H distance was 0.75 Å.

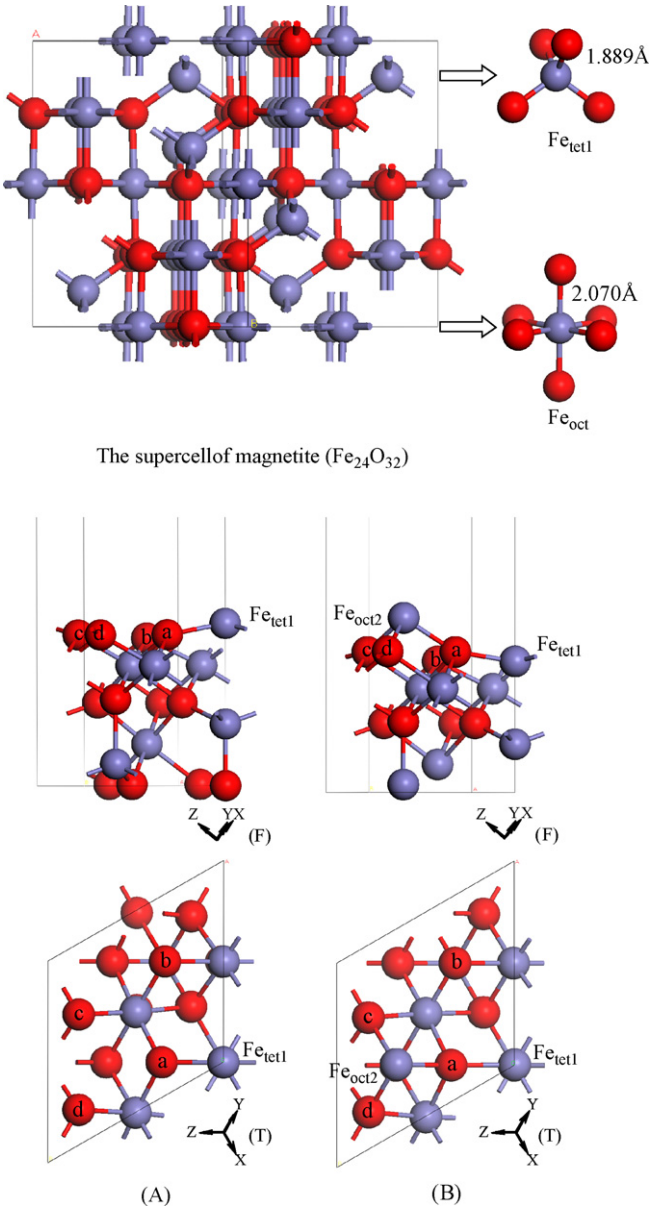

Fig. 1. The supercell of magnetite ($Fe_{24}O_{32}$) and the schematic front (F) and top (T) views for the Fe_{tet1} (a)- and Fe_{oct2} (b)-terminated surfaces in a p(1×1) unit cell of Fe_3O_4(1 1 1) (purple, Fe atom; red, oxygen atom). (For interpretation of the references to color in this figure legend, the reader is referred to the web version of the article.)

3. Results and discussion

3.1. Hydrogen adsorption on the Fe_{tet1}-terminated surface

3.1.1. θ_H = 2/5 ML

As shown in Fig. 2, there are six models (**1**–**6**) for hydrogen adsorbed on the Fe_{tet1}-terminated surface at 2/5 ML, and the computed bond lengths and adsorption energies are also given.

There are two dissociation forms, i.e.; homolytic (**1**–**3**) and heterolytic (**4** and **5**). In **1**–**3**, H_2 dissociates homolytically and form two O–H bonds, while in **4** and **5**, H_2 dissociates heterolytically and forms one O–H bond and one Fe–H bond. **6** has adsorbed molecular hydrogen. The most stable adsorption is **3** followed by **2** (−1.62 eV vs. −1.19 eV), and the least stable adsorption is **6** (−0.21 eV). Compared to **2**, the strongest adsorption of **3** can be attributed to the shortest distances of non-bond electrostatic interaction between the adsorbed hydrogen and the second nearest neighboring oxygen

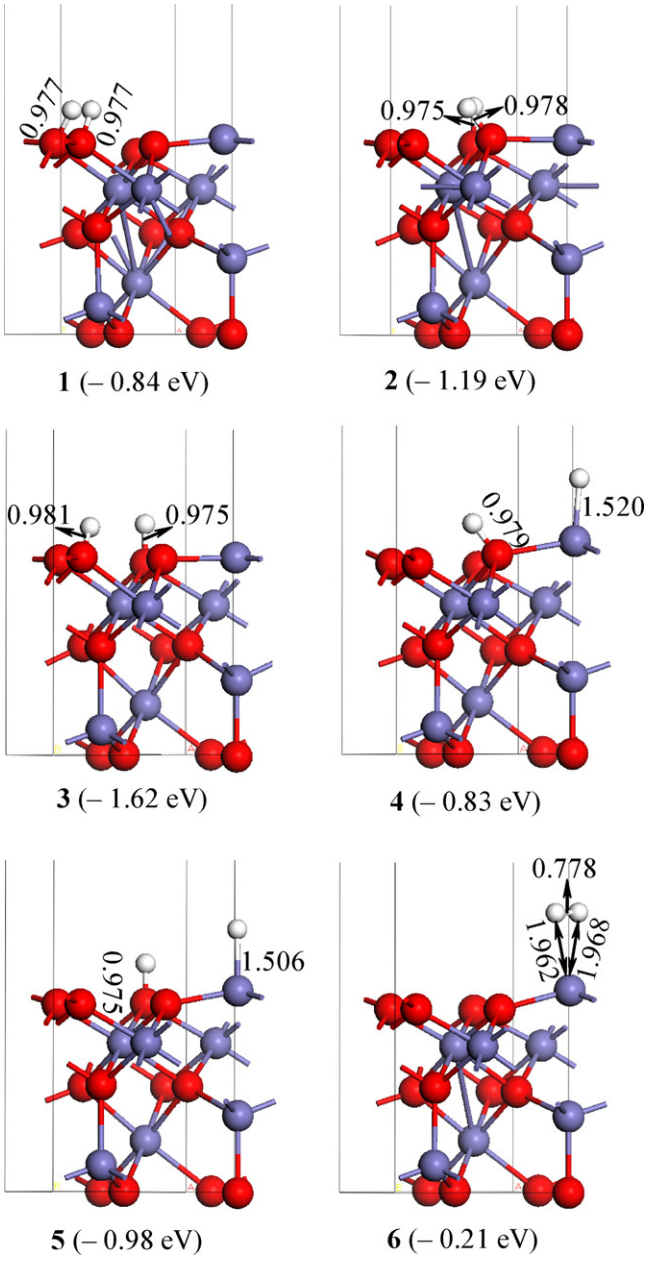

Fig. 2. Hydrogen adsorption on the Fe_{tet1}-terminated Fe_3O_4(1 1 1) surface at 2/5 ML (purple, Fe atom; red, oxygen atom; white, hydrogen atom). (For interpretation of the references to color in this figure legend, the reader is referred to the web version of the article.)

atoms. For example, the distances of the non-bond interaction between the H and O atoms in **3** are 2.211–2.214 Å, while those are 2.298–2.388 Å in **2**. Therefore, the most stable site may have the higher coordination. It should be noted, though, that the strength of an adsorption site is not necessarily related to bond length.

3.1.2. θ_H = 4/5 ML

Fig. 3 shows the hydrogen adsorption modes on the Fe_{tet1}-terminated surface at 4/5 ML (**7**–**9**) along with the computed bond lengths and adsorption energies.

In **7** and **8**, there are three O–H bonds and one Fe–H bond representing one homolytic and one heterolytic H_2 dissociation, while there are four O–H bonds in **9** representing two homolytic H_2 dissociations. **7** can be considered as the superposition of **1** and **4**, and **8** as that of **3** and **4**. **9** is the combination of **1** and **2**. On the basis of the results, it is to expect that **9** should be thermodynamically more favorable than **7** and **8**. As shown in Fig. 3, **9** is indeed more stable than **7** and **8**, but in much less extent. The difference between **9** and **8** is only 0.06 eV. These rather smaller adsorptions of **7**–**9** can be explained by the repulsive effect of the dissociatively adsorbed hydrogen atoms; for example, the shortest distances among these hydrogen atoms are 1.926–2.448 Å.

3.1.3. Electronic structure

Since **3** and **5** represent the most stable homolytic and heterolytic dissociation adsorption models at 2/5 ML on the Fe_{tet1}-terminated surface, respectively, the local density of states (LDOS) for the adsorbed H atoms and the surface Fe and O atoms was calculated to understand the bonding nature between H and Fe_3O_4(1 1 1).

Fig. 4a shows the LDOS for the homolytic dissociation adsorption model (**3**). The surface H_{Ob} and H_{Od} have two very weak peaks; the first one at −9.0 eV is the energy level for the 1s orbital, and the second one at −21.0 eV is contributed by the oxygen 2s orbital [47]. After adsorption, both the 2s and 2p orbitals of the surface oxygen shift to lower energy levels. For the heterolytic dissociation adsorption model (**5**), the LDOS for the O–H bond is approximately the same as in case of **3**, while that of the Fe–H bond is somewhat complicated. For the surface hydrogen, the energy level has two peaks, one is the 1s orbital (−3.7 eV) and the second one above the Fermi level is contributed by the 3d orbital of Fe. For the surface Fe, significant shifts of the energy level have been found for the 3d orbital, and that of the 4s orbital is rather weak. It shows clearly that the 2s and 2p orbitals of oxygen and the 3d orbital of iron are responsible for the O–H and Fe–H bonding, respectively.

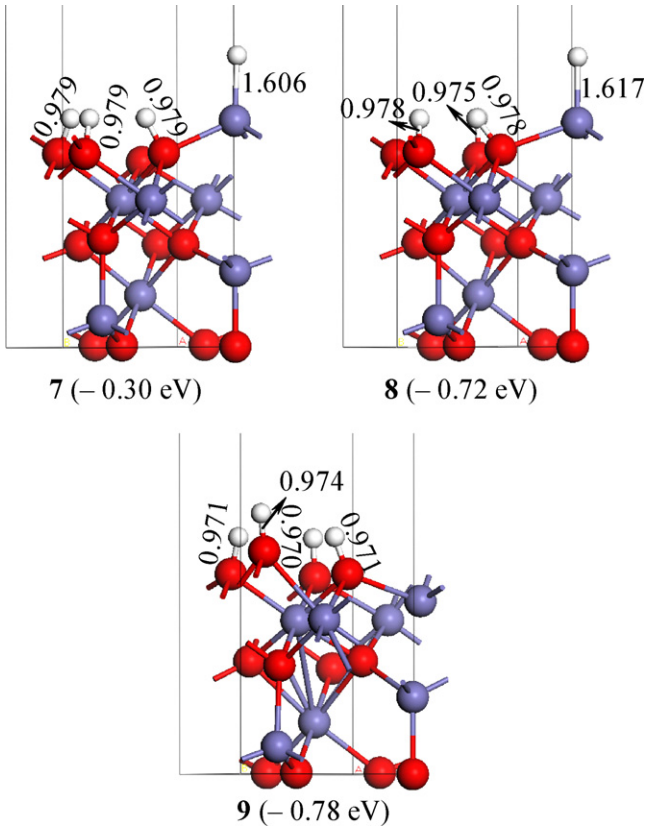

Fig. 3. Hydrogen adsorption on the Fe_{tet1}-terminated Fe_3O_4(1 1 1) surface at 4/5 ML (purple, Fe atom; red, oxygen atom; white, hydrogen atom). (For interpretation of the references to color in this figure legend, the reader is referred to the web version of the article.)

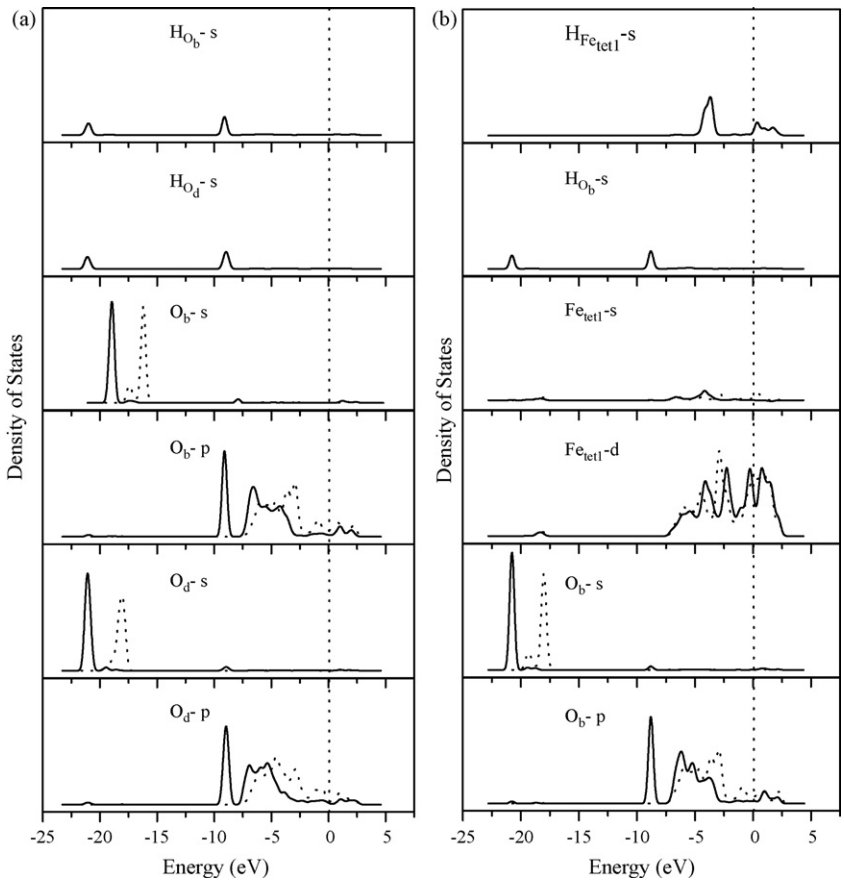

Fig. 4. LDOS for adsorbed H and surface Fe/O atoms in **3** (a) and **5** (b) on the Fe_{tet1}-terminated Fe_3O_4(1 1 1) surface at 2/5 ML: H_{Fetet1} on the top of Fe_{tet1} atom; H_{Ob} on the top of O_b atom (solid lines for bands after adsorption, dotted lines for bands before adsorption).

3.2. Hydrogen adsorption on the Fe_{oct2}-terminated surface

3.2.1. θ_H = 1/3 ML

Fig. 5 shows the adsorption models on the Fe_{oct2}-terminated surface at 1/3 ML (**10**–**13**), and the calculated bond lengths and adsorption energies also are given.

In **10**, molecular H_2 adsorbs on the top of Fe_{oct2} and the computed adsorption energy is −0.66 eV. In **11–13**, H_2 adsorbs dissociatively and heterolytically on surface Fe and O atoms. **11** has the largest adsorption energy (−1.21 eV), while those of **12** and **13** are much smaller (−0.55 and −0.20 eV, respectively). In contrast to **10** and **11**, strong surface reconstructions have been found in **12** and **13**.

The diagram of the lowest energy molecular orbital of O–H bond in **3** and Fe–H bond in **11** are given in Fig. 6. Along with the charge distribution, the O–H and Fe–H bond have polarized and covalent nature. In the homolytic dissociation of **3**, H has the same charge (+0.44 and +0.45), while H has the different charge (−0.30 and +0.45) in the heterolytic dissociation of **11**.

3.2.2. θ_H = 2/3 ML

Fig. 7 shows the adsorption modes on the Fe_{oct2}-terminated surface at 2/3 ML (**14**–**20**), and the computed bond lengths and adsorption energies also are displayed.

As shown in Fig. 7, **14**–**16** have one adsorbed molecular H_2 and one dissociatively adsorbed H_2 in homolytic (**16**) or heterolytic (**14** and **15**) forms. They have very close adsorption energies (−0.32 to −0.37 eV) despite their different structures. Apart from the terminal Fe–H bonds, there is one hydrogen atom bridging bond in **15**, in which the hydrogen atom bridges Fe_{tet1} and Fe_{oct2} forming one Fe–H–Fe bond (1.738 and 1.739 Å).

In contrast to **14**–**16**, **17**–**20** have only dissociatively adsorbed H_2. In **17** and **18**, there are two O–H bonds, as well as one terminal Fe–H bond and one bridging Fe–H–Fe bonds. In **19**, there are three O–H bonds and one terminal Fe–H bond, while there are three O–H bonds and one bridging Fe–H–Fe bond in **20**. The adsorption energy (−0.35 eV) of **18** is close to those of **14**–**16**, while those of **17**, **19** and **20** are somewhat smaller. Compared to **11**, the hydrogen adsorption energies become smaller when increasing the H_2 coverage.

3.2.3. θ_H = 1 ML

There are merely three models for hydrogen adsorbed on the Fe_{oct2}-terminated surface at 1 ML. The computed bond lengths and adsorption energies are displayed in Fig. 8.

As shown in Fig. 8, the constructed structures seem more complicated due to that the Fe atoms and some O atoms leave their original positions, as compared to Fig. 1. There are activated H_2 adsorbed on Fe_{oct2} in both **21** and **22**. Interestingly, a third H dissociatively adsorbs on Fe_{oct2} in **21** with a Fe–H bond length of 1.542 Å. Compared to **22**, **23** has an H atom bridging Fe_{oct2} and Fe_{tet1} yielding the corresponding Fe_{oct2}–H–Fe_{tet1} bond. The computed adsorption energies of **21**–**23** are −0.32, −0.30 and −0.24 eV, respectively, and these energies are close to those of **14**–**19**.

3.2.4. Electronic structure

Fig. 9 shows the LDOS analysis of the adsorbed H atoms on the Fe_{oct2}-terminated Fe_3O_4(1 1 1) surface (**11**). As expected that there is no difference between those of the O–H bond in **11** and **3** as well as **5** (Fig. 4). However, there are significant differences between the d

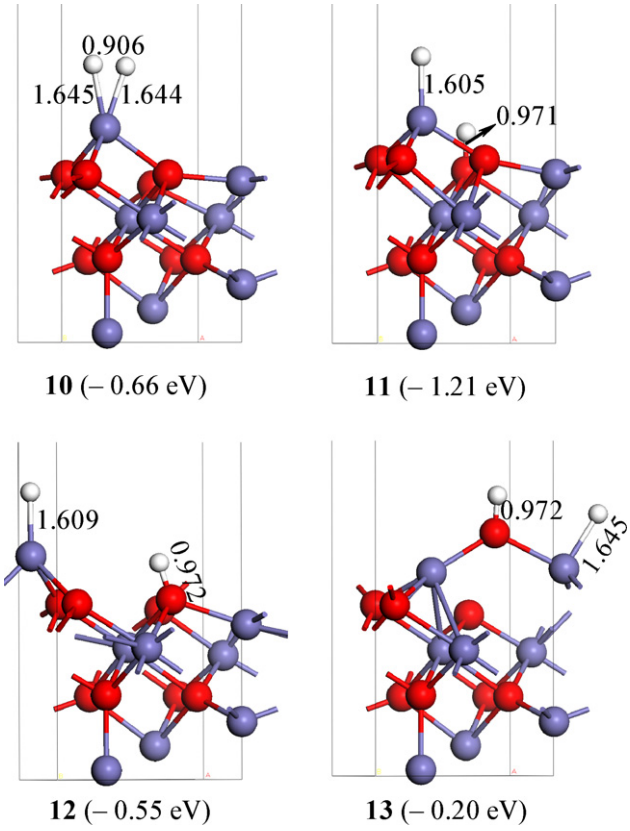

Fig. 5. Hydrogen adsorption on the Fe_{oct2}-terminated Fe_3O_4(1 1 1) surface at 1/3 ML (purple, Fe atom; red, oxygen atom; white, hydrogen atom). (For interpretation of the references to color in this figure legend, the reader is referred to the web version of the article.)

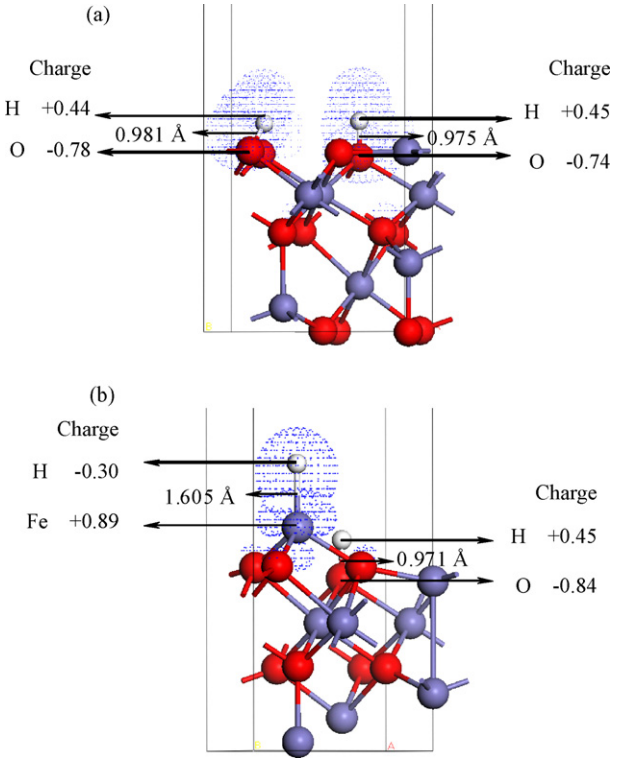

Fig. 6. Schematic diagram of molecular orbital: (a) **3** with homolytic dissociation (two O–H bonds are shown). (b) **11** with heterolytic dissociation (only Fe–H bonding is shown, and the O–H bonding is similar with those in(a)).

orbitals of Fe_{oct2} and Fe_{tet1} centers and also between the s orbital of hydrogen bonded to Fe_{oct2} and Fe_{tet1}. The surface H_{Feoct2} has three weak peaks; one at −1.3 eV is the energy level of the 1s orbital, the others at −2.9 and −4.0 eV maybe due to the split iron 3d orbital. For surface Fe_{oct2}, there is obvious change of the 3d orbital respect to the bare surface, while that of 4s orbital is weak. The O–H and Fe–H bonds in **11** have the same characteristic as in **3** and **5**.

Generally, there are no significant changes of the LDOS for the same type of bonds upon increasing coverage. Significant changes are found for different adsorption types, e.g.; chemisorption and physisorptrion. For considering the coverage effect, we

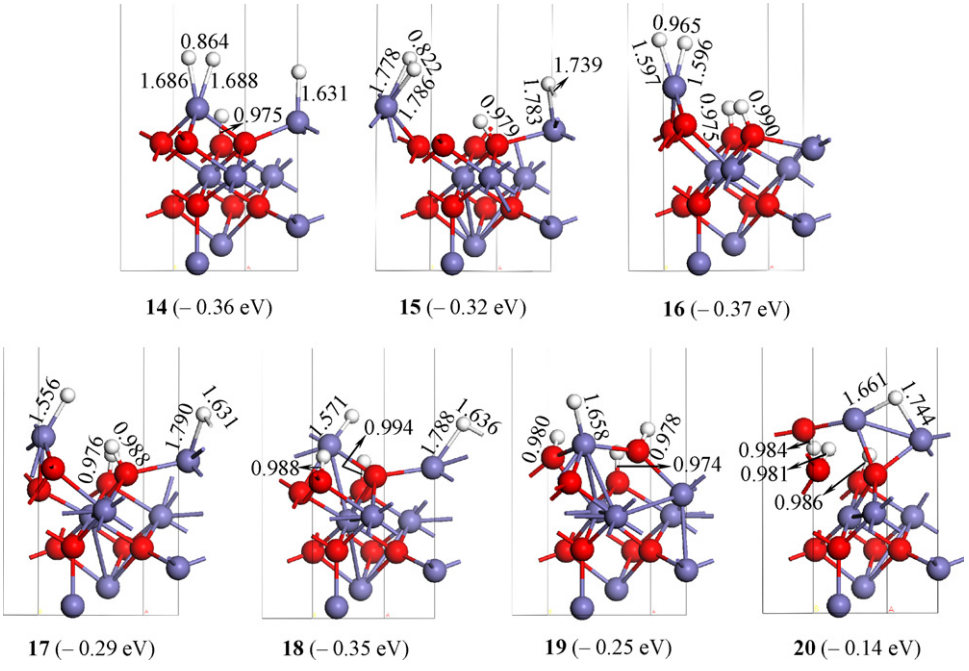

Fig. 7. Hydrogen adsorption on the Fe_{oct2}-terminated Fe_3O_4(1 1 1) surface at 2/3 ML (purple, Fe atom; red, oxygen atom; white, hydrogen atom). (For interpretation of the references to color in this figure legend, the reader is referred to the web version of the article.)

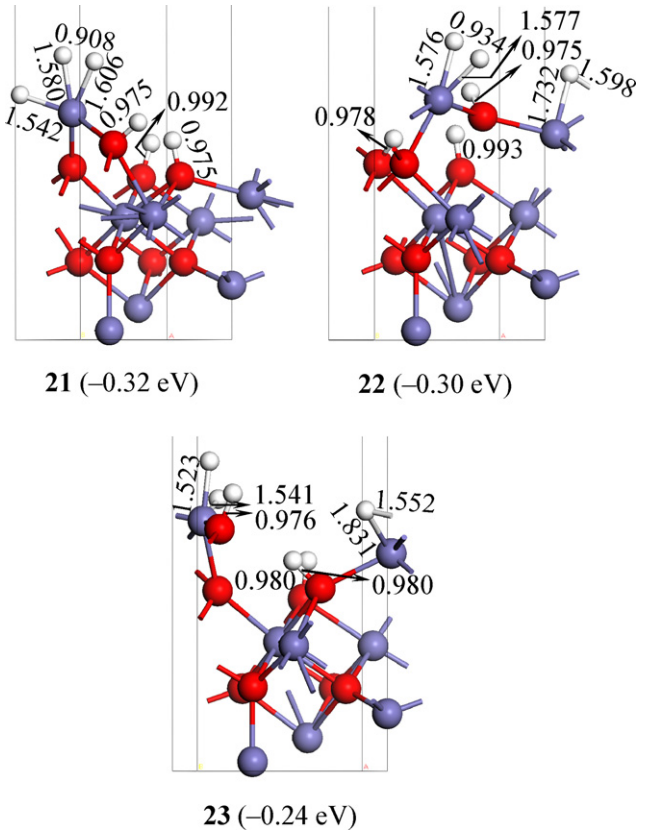

Fig. 8. Hydrogen adsorption on the Fe_{oct2}-terminated Fe_3O_4(1 1 1) surface at 1 ML (purple, Fe atom; red, oxygen atom; white, hydrogen atom). (For interpretation of the references to color in this figure legend, the reader is referred to the web version of the article.)

have calculated the LDOS for Fe_{tet1}-(a) and Fe_{oct2}-(b) terminated Fe_3O_4(1 1 1) surface at low and high coverage, respectively. For the Fe_{tet1}-terminated surface, we choose **3** at 2/5 ML and **9** at 4/5 ML, while for the Fe_{oct2}-terminated surface, **10** and **11** at 1/3 ML are selected for comparing the LDOS of H–Fe and H–O bond with that of **16** at 2/3 ML, respectively. That is, there is additional dissociated H_2 on two surface oxygen atoms in **16** comparing with **10**, while comparing with **11**, **16** has one more dissociated H atom on Fe and O atom, respectively. As shown in Fig. 10, there are little shifts for all orbital bands at high coverage comparing with the low coverage.

3.3. Discussion

As shown in Fig. 2, the most stable adsorption of hydrogen on the Fe_{tet1}-terminated Fe_3O_4(1 1 1) surface at 2/5 ML is the homolytically dissociatively adsorbed **3** (−1.62 eV), while that of heterolytically dissociatively adsorbed states and molecular hydrogen are less stable. With the increase of the hydrogen coverage at 4/5 ML, there are three adsorption modes with both homolytically and heterolytically adsorbed H or with homolytically adsorbed H in very close energy, indicating the possibility of the co-existence and equilibrium of several adsorption modes.

On the Fe_{oct2}-terminated Fe_3O_4(1 1 1) surface at 1/3 ML, the most stable hydrogen adsorption is the heterolytically dissociatively adsorbed **11** (−1.21 eV), while that of other heterolytically dissociatively adsorbed states and molecular hydrogen are less stable. With the increase of hydrogen the coverages at 2/3 and 1 ML, both dissociatively adsorbed hydrogen and molecular hydrogen become possible, and the most interesting aspect is the formation of bridging hydrogen bond over two Fe centers (Fe_{tet1} and Fe_{oct2}).

Although both terminations of the Fe_3O_4(1 1 1) surface is proposed to be the most stable one in experiment and theory, the Fe_{tet1}-terminated surface has greater hydrogen adsorption energies than the Fe_{oct2}-terminated one. However, the reverse trend is found for CO adsorption [29], and CO adsorption on the Fe_{oct2}-terminated surface is more stable than on the Fe_{tet1}-terminated surface.

Since iron, iron oxides and iron carbides are used as catalysts, it is interesting to compare the adsorption of hydrogen on the different surfaces, as summarized in Table 1. For hydrogen adsorption, the Fe(1 1 0) surface is most active, followed by the Fe(1 1 1) and Fe(1 0 0) surfaces, as found both experimentally [51,53,54] and theoretically [32,49,50,52].

The hydrogen adsorption energies on the metallic Fe_3C(0 1 0) [55] and Fe_5C_2(1 0 0) [33] surfaces are close to that on the Fe(1 1 0) surface, indicating their similarity. However, carbon-containing surfaces, like Fe_5C_2(0 0 1) and Fe_3C(1 0 0), are more active for hydrogen adsorption than metallic surfaces. This reveals that carbon-containing surfaces of iron carbides have stronger hydrogen adsorption ability than pure or metallic iron surfaces in FTS, in agreement with the observation that TiC(1 1 1) has stronger activation ability of hydrogen than pure Ti [48].

It is also to note that the Fe_{tet1}-terminated Fe_3O_4(1 1 1) surface has the strongest hydrogen adsorption energy, as compared to the Fe_5C_2(0 0 1) surface, while the Fe(1 1 0) has the smallest hydrogen

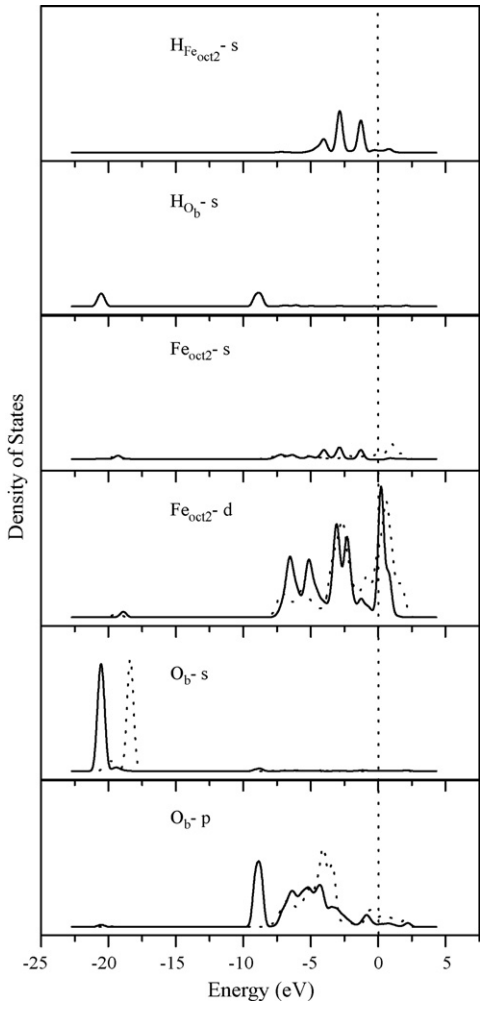

Fig. 9. LDOS for adsorbed H and surface Fe/O atoms in **11** on the Fe_{oct2}-terminated Fe_3O_4(1 1 1) surface at 1/3 ML: H_{Feoct2} on the top of Fe_{oct2} atom; H_{Ob} on the top of O_b atom (solid lines for bands after adsorption, dotted lines for bands before adsorption).

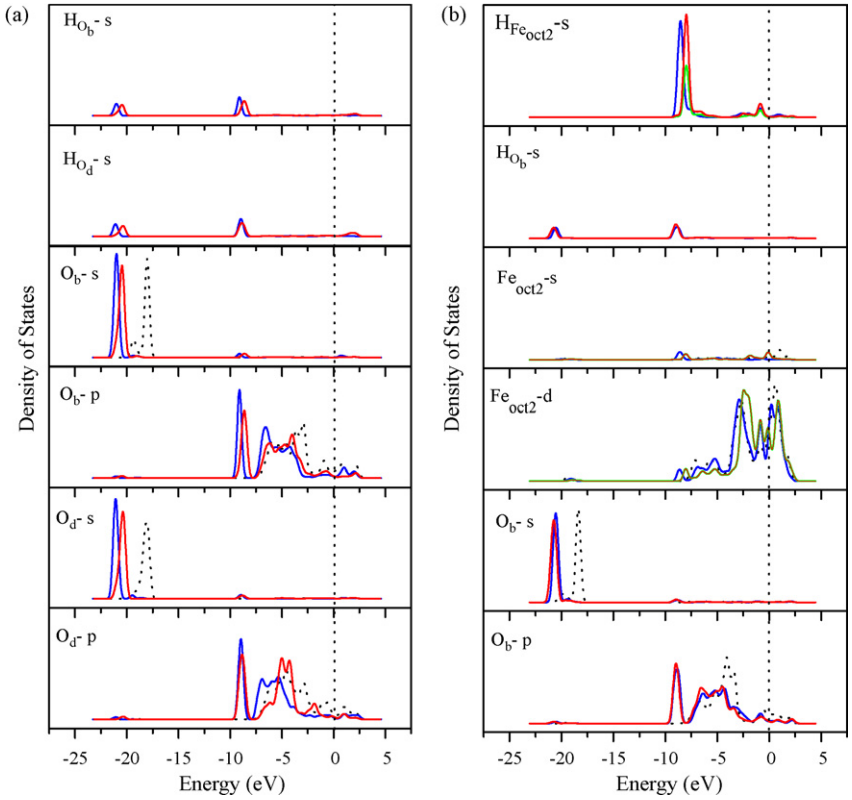

Fig. 10. LDOS for the Fe_{tet1}-(a) and Fe_{oct2}-(b) terminated Fe_3O_4(1 1 1) surfaces at low and high coverages. (a) Blue lines, **3** at 2/5 ML; red lines, **9** at 4/5 ML; dotted lines, before adsorption. (b) Blue lines, **10** at 1/3 ML; green lines, **11** at 1/3 ML; red lines, **16** at 2/3 ML; dotted lines, before adsorption. (For interpretation of the references to color in this figure legend, the reader is referred to the web version of the article.)

Table 1
The largest adsorption energies for H_2 on different surfaces of iron metal (Fe), iron carbides (Fe_5C_2 and Fe_3C) and iron oxide (Fe_3O_4) at low coverage.

	Site		DFT		Exp.
Fe(1 0 0)	4-fold	−0.74 [49][a]	−0.70 [50][b]		−0.74 [51]
Fe(1 1 0)	3-fold	−1.42 [49][a]	−1.39 [52][b]	−1.06 [49][c]	−1.05 [53]
Fe(1 1 1)	Top-shallow bridge	−1.39 [32][a]		−1.12 [32][c]	−0.91 [54]
Fe_5C_2(1 0 0)	3-fold	−1.50 [33][a]			
Fe_5C_2(0 0 1)	3-fold/CH	−1.56 [33][a]			
Fe_5C_2(1 1 0)	3-fold/CH	−1.44 [33][a]			
Fe_3C(0 1 0)	2-fold		−1.52 [55][b]	−1.06 [55][c]	
Fe_3C(1 0 0)	3-fold/CH		−1.49 [55][b]	−1.20 [55][c]	
Fe_3C(0 0 1)	3-fold/2-fold		−1.27 [55][b]	−0.88 [55][c]	
Fe_3O_{4tert}		−1.62[d]			
Fe_3O_{4oct}		−1.21[d]			

[a] Represent the results which are calculated using PBE.
[b] Represent the results which are calculated using PW91.
[c] Represent the results which are calculated using RPBE.
[d] This work.

adsorption energy. This indicates the enhanced differences of these surfaces in the catalytic reactions and also the complexity of iron-based catalysts.

4. Conclusions

Density functional theory calculations have been carried out to investigate hydrogen adsorption behaviors on two different terminations (Fe_{tet1}- and Fe_{oct2}-termination) of the Fe_3O_4(1 1 1) surface at a series of coverages.

For hydrogen adsorption on the Fe_{tet1}-terminated Fe_3O_4(1 1 1) surface at 2/5 ML, H_2 homolytically and dissociatively adsorbed on surface O atoms shows the higher stability, closely followed by the heterolytically and dissociatively adsorbed states, while the molecular hydrogen adsorption is not competitive. At higher coverage (4/5 ML), the adsorption mode with homolytically adsorbed H and that with both homolytically and heterolytically adsorbed H become close in energy. This rather close energy indicates the possibility of co-existence or equilibrium among these adsorption modes.

For hydrogen adsorption on the Fe_{oct2}-terminated Fe_3O_4(1 1 1) surface at 1/3 ML, atomic H prefers to adsorb on one Fe_{oct2} and one O_b atom with the largest adsorption energy. However, several stable adsorption modes become possible at 2/3 and 1 ML.

Comparing the adsorption on both terminations, H_2 prefers to dissociatively adsorb on the Fe_{tet1}-terminated surface than on the Fe_{oct2}-terminated surface, and this trend is reversed with the CO adsorption on the same surfaces. Such different behaviors have

also been found on the surfaces of iron and iron carbides. These differences reveal the complexity of iron-based catalysts.

Acknowledgments

This work was supported by Chinese Academy of Sciences and the National Natural Science Foundation of China (No. 20873173); and the National Outstanding Young Scientists Foundation of China (No. 20625620).

References

[1] D.M. Lind, S.-P. Tay, S.D. Berry, J.A. Borchers, R.W. Erwin, J. Appl. Phys. 73 (1993) 6886.
[2] M.A.M. Gijs, P.J. Kelly, European Patent Application, EP 0 672 303 A1 (1995).
[3] P.A.A. van der Heijden, P.J.H. Bloemen, J.M. Metselaar, R.M. Wolf, J.M. Gaines, J.T.W.M. van Eemeren, P.J. van der Zaag, W.J.M. de Jonge, Phys. Rev. B 55 (1997) 11569.
[4] Y. Ijiri, J.A. Borchers, R.W. Erwin, S.-H. Lee, P.J. van der Zaag, R.M. Wolf, Phys. Rev. Lett. 80 (1998) 608.
[5] K. Ghosh, S.B. Ogale, S.P. Pai, M. Robson, E. Li, I. Jin, Z.W. Dong, R.L. Greene, R. Ramesh, T. Venkatesan, M. Johnson, Appl. Phys. Lett. 73 (1998) 689.
[6] R. Wiesendanger, I.V. Shvets, D. BuKrgler, G. Tarrach, H.-J. GuKntherodt, J.M.D. Coey, Europhys. Lett. 19 (1992) 141.
[7] J.W. Geus, Appl. Catal. 25 (1986) 313.
[8] K.R.P.M. Rao, F.E. Huggins, V. Mahajan, G.P. Huffman, V.U.S. Rao, B.L. Bhatt, D.B. Bukur, B.H. Davis, R.J. O'Brien, Top. Catal. 2 (1995) 71.
[9] D.S. Newsome, Catal. Rev. Sci. Eng. 21 (1980) 275.
[10] H.B. Zhang, G.L. Schrader, J. Catal. 95 (1985) 325.
[11] D.G. Rethwisch, J.A. Dumesic, J. Catal. 101 (1986) 35.
[12] C.-S. Huang, L. Xu, B.H. Davis, Fuel Sci. Technol. Int. 11 (1993) 639.
[13] C.-S. Huang, B. Ganguly, G.P. Huffman, F.E. Huggins, B.H. Davis, Fuel Sci. Technol. Int. 11 (1993) 1289.
[14] A. Raje, R.J. O'Brien, L. Xu, B.H. Davis, in: C.H. Bartholomew, G.A. Fuentes (Eds.), Catalyst Deactivation 1997, Studies in Surface Science Catalysis, vol. 111, Elsevier, Amsterdam, 1997, p. 527.
[15] S.A. Chambers, S.A. Joyce, Surf. Sci. 420 (1999) 111.
[16] Y. Joseph, W. Ranke, W. Weiss, J. Phys. Chem. B 104 (2000) 3224.
[17] U. Leist, W. Ranke, K. Al-Shamery, Phys. Chem. Chem. Phys. 5 (2003) 2435.
[18] W. Weiss, W. Ranke, Prog. Surf. Sci. 70 (2002) 1.
[19] C. Kuhrs, Y. Arita, W. Weiss, W. Ranke, R. Schlögl, Top. Catal. 14 (2000) 111.
[20] Sh.K. Shaikhutdinov, Y. Joseph, C. Kuhrs, W. Ranke, W. Weiss, Faraday Discuss. 114 (1999) 363.
[21] K. Adib, D.R. Mullins, G. Totir, N. Camillone III, J.P. Fitts, K.T. Rim, G.W. Flynn, R.M. Osgood Jr., Surf. Sci. 524 (2003) 113.
[22] C. Lemire, R. Meyer, V.E. Henrich, Sh.K. Shaikhutdinov, H.-J. Freund, Surf. Sci. 572 (2004) 103.
[23] T. Genger, O. Hinrichsen, M. Muhler, Catal. Lett. 59 (1999) 137.
[24] W. Mokwa, D. Kohl, G. Heiland, Surf. Sci. 99 (1980) 202.
[25] A.L. Dent, R.J. Kokes, J. Phys. Chem. 73 (1969) 3772.
[26] L. Zhu, K.L. Yao, Z.L. Liu, Phys. Rev. B 74 (2006) 035409.
[27] Y.L. Li, K.L. Yao, Z.L. Liu, Surf. Sci. 601 (2006) 876.
[28] R. Pentcheva, F. Wendler, H.L. Meyerheim, W. Moritz, N. Jedrecy, M. Scheffler, Phys. Rev. Lett. 94 (2005) 126101.
[29] D.-M. Huang, D.-B. Cao, Y.-W. Li, H. Jiao, J. Phys. Chem. B 110 (2006) 13920.
[30] M.E. Grillo, M.W. Finnis, W. Eanke, Phys. Rev. B 77 (2008) 075407.
[31] T. Yang, X.-D. Wen, C.-F. Huo, Y.-W. Li, J.G. Wang, H. Jiao, J. Phys. Chem. C 112 (2008) 6372.
[32] (a) C.-F. Huo, Y.-W. Li, J. Wang, H. Jiao, J. Phys. Chem. B 109 (2005) 14160;
(b) Z.-Y. Ma, C.-F. Huo, X.-Y. Liao, Y.-W. Li, J. Wang, H. Jiao, J. Phys. Chem. C 111 (2007) 4305;
(c) C.-F. Huo, J. Ren, Y.-W. Li, J. Wang, H. Jiao, J. Catal. 249 (2007) 174.
[33] D.-B. Cao, F.-Q. Zhang, Y.-W. Li, J. Wang, H. Jiao, J. Phys. Chem. B 109 (2005) 833.
[34] (a) M.C. Payne, D.C. Allan, T.A. Arias, J.D. Joannopoulos, Rev. Mod. Phys. 64 (1992) 1045;
(b) V. Milman, B. Winkler, J.A. White, C.J. Pickard, M.C. Payne, E.V. Akhmataskaya, R.H. Nobes, Int. J. Quant. Chem. 77 (2000) 895.
[35] (a) J.P. Perdew, A. Zunger, Phys. Rev. B 23 (1981) 5048;
(b) J.P. Perdew, J.A. Chevary, S.H. Vosko, K.A. Jackson, M.R. Pederson, D.J. Singh, C. Fiolhais, Phys. Rev. B 46 (1992) 6671.
[36] J.A. White, D.M. Bird, Phys. Rev. B 50 (1994) 4954.
[37] D. Vanderbilt, Phys. Rev. B 41 (1990) 7892.
[38] H.J. Monkhorst, J.D. Pack, Phys. Rev. B 13 (1976) 5188.
[39] S.G. Louie, S. Froyen, M.L. Cohen, Phys. Rev. B 26 (1982) 1738.
[40] (a) S.K. Nayak, M. Nooijen, S.L. Bernasek, J. Phys. Chem. B 105 (2001) 164;
(b) H.S. Cheng, D.B. Reiser, S.W. Dean Jr., K. Baumert, J. Phys. Chem. B 105 (2001) 12547;
(c) Q. Ge, S.J. Jenkins, D.A. King, Chem. Phys. Lett. 327 (2000) 125.
[41] R.W.G. Wyckoff, Crystal Structures, vol. 2, 2nd ed., Interscience Publishers, New York, 1982, p. 5.
[42] N.D. Spencer, R.C. Schoonmaker, G.A. Somorjai, J. Catal. 74 (1982) 129.
[43] H. Topsøe, J.A. Dumesic, M. Boudart, J. Catal. 28 (1973) 477.
[44] J. Ahdjoudj, C. Martinsky, C. Minot, M.A. Van Hove, G.A. Somorjai, Surf. Sci. 443 (1999) 133.
[45] (a) N.G. Condon, P.W. Murray, F.M. Leibsle, G. Thornton, A.R. Lennie, D.J. Vaughan, Surf. Sci. 310 (1994) L609;
(b) S.K. Shaikhutdinov, M. Ritter, X.-G. Wang, H. Over, W. Weiss, Phys. Rev. B 60 (1999) 11062;
(c) M. Ritter, W. Weiss, Surf. Sci. 432 (1999) 81.
[46] W. Moritz, R. Imbihl, R.J. Behm, G. Ertl, T. Matsushima, J. Chem. Phys. 83 (1985) 1959.
[47] Such phenomena have also been found in the LDOS of HF and H_2O.
[48] W.A. Herrmann, Angew. Chem. Int. Engl. 21 (1982) 117.
[49] D.E. Jiang, E.A. Carter, Phys. Rev. B 70 (2004) 064102.
[50] M. Eder, K. Terakura, J. Hafner, Phys. Rev. B 64 (2001) 115426.
[51] M.L. Burke, R.J. Madix, Surf. Sci. 237 (1990) 20.
[52] D.E. Jiang, E.A. Carter, Surf. Sci. 547 (2003) 85.
[53] E.A. Kurz, J.B. Hudson, Surf. Sci. 195 (1988) 15.
[54] S.L. Bernasek, M. Zappone, P. Jiang, Surf. Sci. 272 (1992) 53.
[55] X.-Y. Liao, S.-G. Wang, Z.-Y. Ma, Y.-W. Li, J. Wang, H. Jiao, J. Mol. Catal. A 292 (2008).